Topological pumping in origami metamaterials

Shuaifeng Li,[1,2] Panayotis G. Kevrekidis,[3] Xiaoming Mao,[2] and Jinkyu Yang[4]
[1]*Department of Aeronautics and Astronautics, University of Washington, Seattle, Washington 98105, USA*
[2]*Department of Physics, University of Michigan, Ann Arbor, Michigan 48109, USA*
[3]*Department of Mathematics and Statistics, University of Massachusetts, Amherst, Massachusetts 01003, USA*
[4]*Department of Mechanical Engineering, Seoul National University, Seoul 08826, Republic of Korea*

(Received 29 January 2024; revised 15 July 2024; accepted 19 July 2024; published 12 August 2024)

We present a mechanism of topological pumping in origami metamaterials with spatial modulation by tuning the rotation angles. Through coupling spatially modulated origami chains along an additional synthetic dimension, the pumping of waves from one topological edge state to another is achieved, where the Landau-Zener transition is demonstrated by varying the number of coupled origami chains. In addition, the inherent nonlinearity of origami metamaterials enables the excitation-dependent Landau-Zener tunneling probability. Furthermore, with the increase of nonlinearity, the topological states tend to localize in several regions in a way reminiscent of discrete breathers. Our findings pave the way towards interband transitions and associated topological pumping features in origami metamaterials.

DOI: 10.1103/PhysRevB.110.075123

I. INTRODUCTION

Topological metamaterials have had a remarkable recent impact not only in condensed matter physics, but also through wave manipulation in photonics and phononics, underpinned by the robustness to imperfections [1–5]. A recent research direction has focused on the higher-dimensional topological effects in lower-dimensional systems by exploiting synthetic dimensions in the parameter space [6–9]. Among these pursuits, Thouless pumping stands out as a captivating demonstration of topological phenomena, offering a dynamic counterpart to the two-dimensional quantum Hall effect and enabling transport behaviors of topological states. Thouless pumping in photonics [10–13], acoustics [14–16], and elasticity [17–22] not only illuminates the topological aspects of dynamic evolution, but also highlights its significance in unraveling the higher-dimensional topological physics; see also the recent review [23].

Meanwhile, recently, the ancient art of origami, with its intricate paper-folding techniques, has captured the interest of the physics and engineering communities [24–26]. Origami metamaterials, comprising an assemblage of origami blocks, offer a unique repertoire of static properties and the dynamic characteristics that hold the promise of mitigating impacts and controlling vibrations [27–30]. Notably, origami metamaterials have been proven to demonstrate the potential for the realization of systems of relevance to condensed matter physics, particularly in the exploration of topological states [31–33]. Origami metamaterials, coupled with their distinct mechanical properties being tuned through initial configurations, position them as convenient platforms for the realization of Thouless pumping, thus opening up intriguing possibilities. Additionally, while most studies on band topology are conducted in linear systems, there is growing interest in the investigation of properties in the presence of nonlinearities [34–37]. Therefore, the intrinsic nonlinearity in origami offers opportunities for investigating the interplay between nonlinearity and topological pumping in elastic systems, which warrants further study.

In this work, we demonstrate topological Thouless pumping in an origami metamaterial consisting of coupled Kresling origami chains, each tailored with modulated geometrical parameters. By engineering the initial rotation angles of the origami units according to the Aubry-André-Harper (AAH) model [38,39], we find nontrivial topological edge states in a single origami chain. Leveraging an additional parameter as a synthetic dimension, we realize the Landau-Zener transition [40,41] and topological pumping in the two-dimensional system with coupled modulated origami chains. Furthermore, our exploration reveals that the nonlinearity of origami can result in asymmetrical Landau-Zener tunneling in a way reminiscent of (but distinctive from) cold-atom experiments [42], and also lead to the transition from topological pumping to discrete breathers [43] and bulk states. Our work not only achieves topological pumping in origami metamaterials, but also delves into the profound influence of nonlinearity thereon.

II. DESIGN OF ORIGAMI METAMATERIALS

We consider the Kresling origami as the unit cell in the origami metamaterials, the geometry of which is shown in Figs. 1(a) and 1(b). The geometric and mechanical parameters for Kresling origami are detailed in the Supplemental Material [44]. We then design the single Kresling origami chain following the AAH model, the prototypical form of which at the level of a tight-binding model is expressed as

$$E\psi_n = t(\psi_{n+1} + \psi_{n-1}) + \mu\cos(2\pi n\xi + \eta)\psi_n, \qquad (1)$$

where ψ is the wave function, n represents the lattice site, E denotes the energy, t is the hopping amplitude, μ is the modulation amplitude of the on-site potential, ξ controls the periodicity of the modulation, and η is the modulation phase.

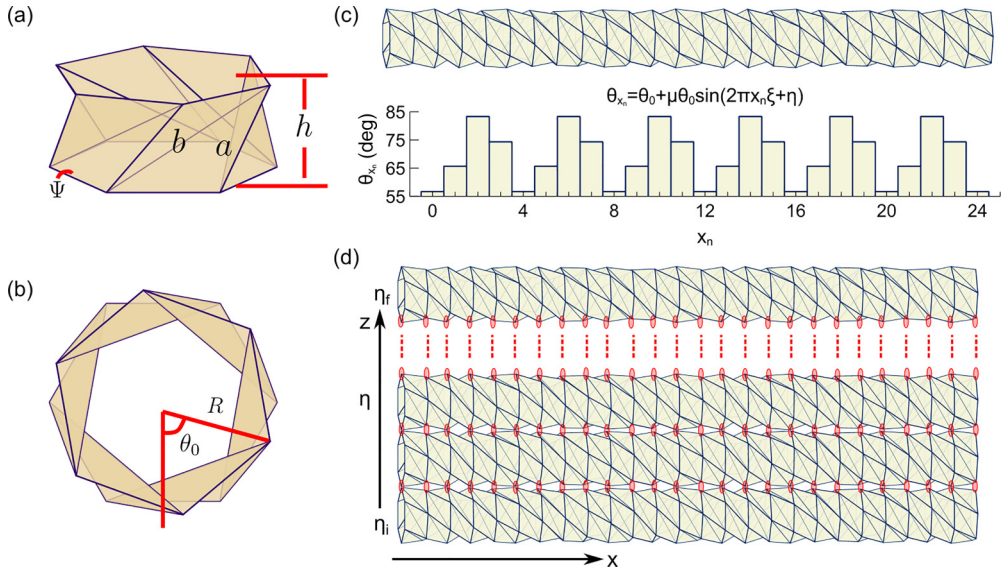

FIG. 1. (a) The side view of Kresling origami. a, b represent lengths of crease lines, and h and Ψ represent the height and folding angle of Kresling origami, respectively. (b) The top view of Kresling origami. θ_0 and R denote the rotation angle between the bottom and top panels, and the radius of Kresling origami, respectively. (c) The side view of the Kresling origami's chain with spatial modulation. The rotation angle of each Kresling origami follows $\theta_{x_n} = \theta_0 + \mu\theta_0 \sin(2\pi x_n\xi + \eta)$. The corresponding values are shown below. (d) The coupled origami chains via torsion springs k_c along a synthetic dimension η. η varies from η_i to η_f. For example, the initial rotation angles of the first chain are $\theta_{x_n} = \theta_0 + \mu\theta_0 \sin(2\pi x_n\xi + \eta_i)$ and those of the last chain are $\theta_{x_n} = \theta_0 + \mu\theta_0 \sin(2\pi x_n\xi + \eta_f)$. The red markers represent the torsion springs.

The on-site potentials of the AAH model, specifically, for the origami chain, the stiffness values, are spatially modulated by the initial rotation angle of Kresling origami $\theta_{x_n} = \theta_0 + \mu\theta_0 \sin(2\pi x_n\xi + \eta)$. Here, μ, ξ, and η represent the modulation amplitude, modulation frequency, and modulation phason (also the synthetic dimension of the system). In our work, we choose 25 Kresling origami elements ($\{x_n \in \mathbb{Z} | 0 \leqslant x_n \leqslant 24\}$), with height $h = 30$ mm, rotation angle $\theta_0 = 70^\circ$, radius $R = 36$ mm, and $\mu = 0.2$. Thus, there are $n = 26$ separators in the single origami chain, each of which has two degrees of freedom (translation u and rotation φ) according to the truss model by considering each crease as a linear spring and the folding of each facet as a linear torsion spring [29,31], where massless trusses and no bending of the chain are considered. Under the configuration with modulation of the initial rotation angles, the truss model indicates that the stiffness will experience a periodic variation, thereby leading to the formulation of the AAH model. More details of the truss model are shown in the Supplemental Material [44].

One of the properties of the AAH model is the fractal nature of its spectrum. To explore this, we show, in the Supplemental Material [44], the spectrum as a function of the parameter ξ and observe a structure known as the Hofstadter butterfly [46]. The Hofstadter butterfly is not only a footprint of the spectral fractality, but also the indicator of a nontrivial band gap whose gap Chern number is conveniently calculated by the integrated density of states (IDS) [47] (see Supplemental Material [44]). In our single Kresling origami chain displayed in Fig. 1(c), we choose $\xi = \frac{1}{4}$ to study the topological states in the nontrivial band gap with the gap Chern number $C_g = -1$, and the rotation angle of each origami in the chain is exhibited in the bottom panel of Fig. 1(c). In this way, this one-dimensional system satisfies the commensurate AAH model and each unit cell contains four origamis. Note that the choices of $\xi = \frac{1}{4}$ and 26 separators in the origami chain (implying 24 periodic separators and 2 additional separators in the boundary) ensure the existence of two bands in the band gap [16,31], which enables the discussion of the Landau-Zener transition below.

The parameter η in the AAH model as an additional degree of freedom is used as a synthetic dimension to construct the two-dimensional origami metamaterials. η linearly varies from η_i to η_f, resulting in the coupled spatially modulated origami chains via torsion springs k_c along the z direction, which induce rotations φ only, as illustrated by Fig. 1(d). z_n denotes the number of coupled origami chains.

To study the dynamical properties of the single Kresling origami chain and the two-dimensional coupled origami chains, we then show the calculated spectra. The Kresling origami has the typical nonlinear behaviors that the stiffness changes under different levels of deformation (see the governing equation and force-displacement curves in the Supplemental Material [44]), which will be detailed later to show its effect on topological pumping. Therefore, to reveal the dispersion topology in such an origami chain, we linearize the governing equation of Kresling origami to obtain linear coefficients (see Supplemental Material [44]). In Fig. 2(a), the eigenspectrum is plotted as a function of η with the clamped boundary condition on both sides of the origami chain. To check if the eigenmodes own features of topological states, the localization index (LI), which is the product of the inverse participation ratio (IPR) and the center of mode (CoM), is used to characterize the localization of energy [31]:

$$\mathrm{LI} = \mathrm{IPR} \times \mathrm{CoM} = |(\boldsymbol{K}\boldsymbol{U}^{\circ 2})^{\circ 2}| \left(\frac{2}{n-2} \boldsymbol{w}^T \boldsymbol{K}\boldsymbol{U}^{\circ 2} \right), \quad (2)$$

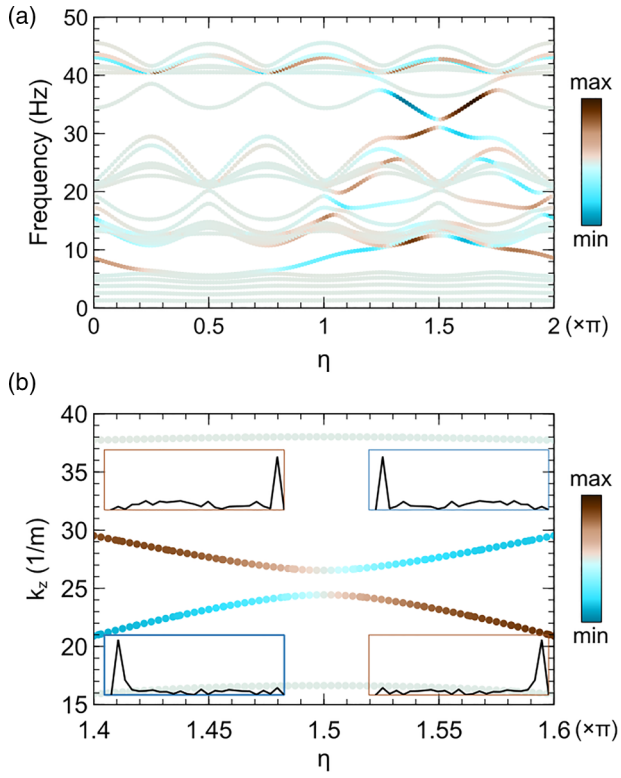

FIG. 2. (a) The calculated eigenspectrum of the single Kresling origami chain as a function of η. (b) The wave number k_z as a function of η for a fixed frequency $f = 40$ Hz. The insets show four eigenmodes (φ) of the origami chain along the x direction, corresponding to $\eta_i = 1.4\pi$ and $\eta_f = 1.6\pi$ of two colored bands, respectively. The color in (a) and (b) represents the localization index, indicating the localization of the energy.

where $\boldsymbol{U}$ is the eigenvector containing translation u and rotation φ, $\boldsymbol{K}$ is the commutation matrix, and $\boldsymbol{w}$ is the weighting vector. $\circ$ denotes the Hadamard product. The clamped boundary condition leads to $n-2$ effective separators. The introduction of LI indicates that if the eigenmode is skewed toward the left (right) boundary, LI is negative (positive). More details including the definition of $\boldsymbol{K}$ and $\boldsymbol{w}$ can be found in the Supplemental Material [44]. According to the color-encoded spectrum in Fig. 2(a), topological edge states with the energy localized on either boundary can be found in the band gap when η is in a certain range.

We choose the topological states within the band gap around 30 Hz when η is between 1.4π and 1.6π to further explore. Therefore, for the two-dimensional origami metamaterials, η linearly varies from $\eta_i = 1.4\pi$ to $\eta_f = 1.6\pi$. Imposing plane-wave harmonic motion along the z direction, variation of wave number k_z shifts the entire spectrum [Fig. 2(a)] by considering slowly varying η along the z direction, resulting in the spectrum $f(\eta, k_z)$, where $k_z \in [0, \frac{\pi}{2R}]$. We then fix the excitation frequency $f(\eta, k_z) = 40$ Hz in the following discussion and generate the relation between k_z and η shown in Fig. 2(b). Topological edge states are illustrated with large |LI| (colored), while the bulk bands are illustrated with small |LI| (gray). Moreover, the eigenmodes (φ) in the insets clearly exhibit the topological edge states with localized energy on either the left end or right end.

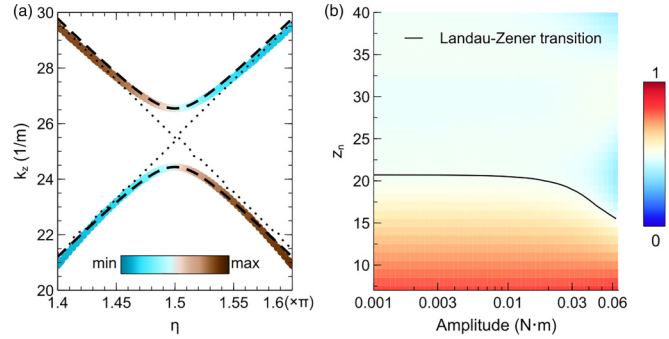

FIG. 3. (a) The close-up view of the relation between k_z and η. The black dashed lines and black dotted lines represent the theoretical adiabatic evolution and diabatic evolution, respectively. (b) The Landau-Zener tunneling probability as a function of number of chains and excitation amplitude. The black solid lines indicate the Landau-Zener transition point, $P_{|\Psi_L\rangle} = 0.5$.

III. LANDAU-ZENER TUNNELING IN ORIGAMI METAMATERIALS

Of particular interest are two bands featuring topological edge states. As depicted in the close-up view in Fig. 3(a), there is a band gap with a size of $\Delta k_z = 2.1$ m^{-1}. This small size of the band gap suggests the sensitivity of topological pumping to the condition of adiabaticity and hence offers a unique opportunity to explore diabatic transition. In the vicinity of $\eta = 1.5\pi$, these two bands can be modeled by a two-level effective Hamiltonian near $k_z = 25.5$ m^{-1} by considering the z direction as time,

$$H(\delta\eta) = \begin{pmatrix} -\alpha\delta\eta & \Delta k_z/2 \\ \Delta k_z/2 & \alpha\delta\eta \end{pmatrix}, \tag{3}$$

where $\alpha = 12.9$ m^{-1} serves as a fitting parameter between the theoretical model and simulation by minimizing the mean-squared error. The bases of H are denoted as $|\Psi_L\rangle$ and $|\Psi_R\rangle$, representing the topological edge states localized at the left and right boundaries, respectively. The eigenvalues of H are illustrated as the black dashed lines in Fig. 3(a), showcasing the excellent agreement with the results from simulation (colored dots). If the initial state is $|\Psi_L\rangle$ at $\eta = 1.4\pi$, residing in the lower level, the final state $|\Psi_f\rangle$ will be a superposition of two topological edge states $|\Psi_L\rangle$ and $|\Psi_R\rangle$. Following the evolution of $|\Psi_L\rangle$, the final state remains localized on the left boundary, corresponding to the diabatic transition (black dotted lines). Alternatively, following the lower level during pumping, the final state will be dominated by $|\Psi_R\rangle$, leading to the localization on the right boundary. Note that the transfer of the topological states is also achieved in the single origami chain mimicking the Su-Schrieffer-Heeger model with time-dependent modulation [31]. The recent progress also shows a system with coupled pendula with Landau-Zener transition in its temporal dynamics [48]. The introduction of a spatial synthetic dimension instead of modulating the origami chain over time provides a practical approach towards transferring topological edge states.

The composition of the final state $|\Psi_f\rangle$ can be predicted by the Landau-Zener model [49], given by $|\Psi_f\rangle = L(z)|\Psi_L\rangle +$

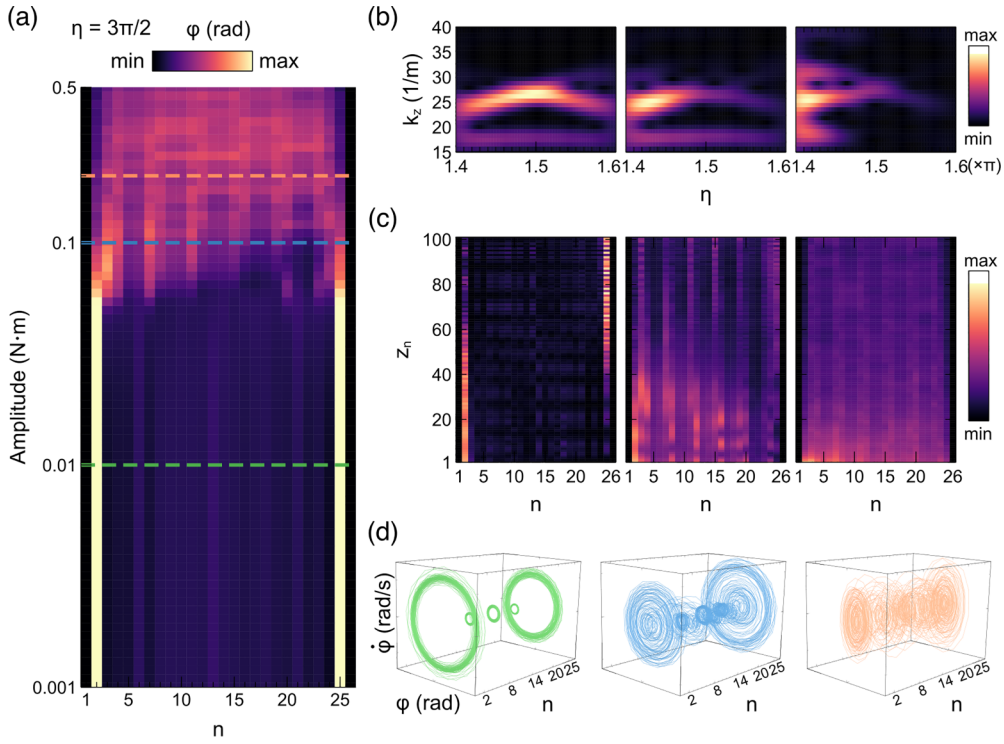

FIG. 4. (a) The rms of φ when $\eta = 3\pi/2$ as a function of excitation amplitude. (b) The spectrogram of the time domain simulation, showcasing the relation between η and k_z. The amplitude of the spectrogram is encoded by color. (c) The rms of φ under different excitation amplitudes. (d) Phase-space representation plot (φ vs $\dot{\varphi}$) at different sites when $\eta = 3\pi/2$. From left to right, the panels in (b)–(d) indicate the cases with increasing excitation amplitudes, corresponding to the dashed lines in (a).

$R(z)|\Psi_R\rangle$, with $L(z)$ and $R(z)$ satisfying the following relation:

$$i\frac{d}{dz}\begin{pmatrix}L(z)\\R(z)\end{pmatrix} = \begin{pmatrix}-\beta z & \Delta k_z/2\\ \Delta k_z/2 & \beta z\end{pmatrix}\begin{pmatrix}L(z)\\R(z)\end{pmatrix}. \tag{4}$$

Here, $\beta = \alpha(\Delta\eta/z_n)$ represents the degree of adiabaticity, which depends on the rate of parameter evolution, $\Delta\eta/z_n$, with $\Delta\eta = 0.2\pi$ being the span of η. By assuming the initial state to be $|\Psi_L\rangle$, the proportion of the final state can be derived as $P_{|\Psi_L\rangle} = L^2(z_n) = e^{-\pi\Delta k_z^2/4\beta}$ and $P_{|\Psi_R\rangle} = R^2(z_n) = 1 - e^{-\pi\Delta k_z^2/4\beta}$. In the Supplemental Material [44], we show $P_{|\Psi_L\rangle}$ as a function of z_n. Therein, when $P_{|\Psi_L\rangle} = 0.5$, the Landau-Zener transition point corresponds to $z_n = 21$. When z_n is sufficiently large, the evolution is slow enough to be adiabatic, resulting in the final state dominated by $|\Psi_R\rangle$. However, when the same process occurs in a system with a smaller z_n, the variation is fast, leading to diabatic behaviors and the final state dominated by $|\Psi_L\rangle$. While the Landau-Zener transition has been realized in photonics and acoustics [13,16], our realization in the elastic platform of Kresling origami fills the blank in elasticity, while naturally posing the challenge of nonlinear extensions thereof.

As mentioned in Sec. I, Kresling origami exhibits intrinsic nonlinearity (see the Supplemental Material [44]). Therefore, we investigate the Landau-Zener tunneling probability calculated by the kinetic energy of the separator as a function of the excitation amplitude. Note that the excitation of the system is through a torque T applied on the separator. As shown in Fig. 3(b), when the excitation amplitude is small and the system remains close to the linear regime with the initial state $|\Psi_L\rangle$ in the lower band, the Landau-Zener transition point ($P_{|\Psi_L\rangle} = 0.5$, black solid line) remains consistent ($z_n = 21$), showing agreement with theoretical results. However, as the amplitude increases to the weakly nonlinear regime, the transition point shifts to the smaller z_n. This suggests that the tunneling probability decreases when the excitation amplitude increases. While previous studies have shown that in the presence of nonlinearity the tunneling probability will increase due to the interactions between the particles [42,50,51], our results show the opposite case, which may result from the strain softening behaviors of Kresling origami. Note that the discussion is only limited in the weakly nonlinear regime because larger excitation amplitude beyond the limit as presented will eliminate topological states, which will be shown below.

IV. TRANSITION OF TOPOLOGICAL PUMPING

To further explore the nonlinear effects of origami on the topological pumping, we excite the system with varying amplitudes from the left boundary to obtain the initial state $|\Psi_L\rangle$ in the lower band. We also fix $z_n = 101$ to ensure the adiabatic evolution, resulting in the final state being predominantly composed of $|\Psi_R\rangle$.

In Fig. 4(a), we show the root mean square (rms) of the field distribution (φ) of the 51st origami chain (middle chain), where $\eta = 3\pi/2$, as a function of excitation amplitude. Evidently, when the amplitude is small (near the linear regime), topological states can be successfully transferred from the left

to the right boundary with the minimal involvement of the bulk states. To illustrate the adiabatic nature of the pump, we employ a time-frequency analysis (spectrogram) to represent the rotational displacement field in the reciprocal space $\hat{\varphi}(\eta, k_z, k_x, f)$. For visualization purposes, $f = 40$ Hz and the rms along the k_x dimensions is taken, which produces $\hat{\varphi}(\eta, k_z)$. As shown in the first panel of Fig. 4(b), when the amplitude is 0.01 N m, the wave is initially distributed around wave numbers k_z corresponding to the excited left-localized topological state. Along the synthetic dimension η, it closely follows the evolution of the lower band. At the end of the process, the majority of the energy is concentrated on the right-localized mode, with a portion scattered to neighboring bulk states. The corresponding rms of φ is shown in the first panel of Fig. 4(c), providing a clear depiction of the topological pumping. In addition, the phase-space representation [$\varphi(t)$ vs $\dot{\varphi}(t)$] is displayed in the first panel of Fig. 4(d) for several separators along the 51st origami chain, showcasing periodic orbits in the phase space. At small amplitude, these mainly involve such orbits at the two boundaries.

As the excitation amplitude continues to rise, the influence of nonlinearity becomes prominent. Gradually, the dominance of topological pumping wanes, resulting in the lesser confinement on the boundary. As shown in Fig. 4(a), the excited waves bypass the boundary-induced confinement and explore more widely in the configuration space of the system. As an example, indicated by the blue dashed line, when the amplitude reaches 0.1 N m, $\hat{\varphi}(\eta, k_z)$ is shown in the second panel of Fig. 4(b). In comparison to the linear case, it becomes evident that the energy is not primarily concentrated on the right-localized mode by the end of the evolution. The rms of φ is displayed in the second panel of Fig. 4(c), revealing the emergence of localized states reminiscent of discrete breathers [43], principally located at certain sites (3rd, 7th, ..., 23rd separators). These modes have certain frequencies located at the band gap (in line with what is expected based on their spatial localization). Further analysis of the subharmonic effect can be found in the Supplemental Material [44]. Likewise, the phase-space representation is illustrated in the second panel of Fig. 4(d). Compared with the linear case, the trajectories show nonlinear features on the periodic orbits and the corresponding excitation of larger amplitude orbits in the bulk of the system. We note that similar transitions from topological states to discrete breathers have also been observed in the one-dimensional spatially modulated nonlinear spring chain [52].

If the excitation amplitude is increased further, the influence of nonlinearity becomes increasingly pronounced. The bulk states will be excited, as evidenced by the large amplitude of φ uniformly distributed in the bulk, shown in Fig. 4(a), when the amplitude is 0.2 N m, marked by the orange dashed line. The third panel of Fig. 4(b) and additional details in the Supplemental Material [44] further confirm that a significant portion of the energy is scattered to the bulk, at 40 Hz and other frequencies. According to the rms of φ in the third panel of Fig. 4(c), the characteristic feature of discrete breathers, where energy is localized at specific sites, becomes less apparent. Instead, the bulk of the system experiences a progressively more uniform excitation. In stark contrast to the previous cases, the relation between φ and $\dot{\varphi}$ exhibits highly nonlinear features, exploring the full phase space and significantly deviating from well-defined periodic orbits, as displayed in the third panel of Fig. 4(d).

In conclusion, our study demonstrates the design of origami metamaterials by coupling spatially modulated Kresling origami chains, following the AAH model, to achieve topological pumping. The intrinsic nonlinearity of origami metamaterials reveals an intriguing phenomenon, characterized by Landau-Zener tunneling probability contingent upon the excitation amplitude (in a way reflecting the system's strain softening nonlinearity). Moreover, as the nonlinearity becomes more pronounced, the topological states gradually transform into spatially localized, temporally periodic states reminiscent of discrete breathers and eventually transition into progressively more uniform bulk states. Our findings provide valuable insights into the evolutionary path from topological pumping to localized, breathing and bulk states in nonlinear systems. These findings inspire experimental explorations and potential applications in origami-based architectures for the manipulation of elastic waves and robust transfer of energy since the parameters used in the simulations are from previous experimental work [31], and the exploration of Landau-Zener-Stückelberg interferometry as well as the corresponding nonlinear features [49,53].

ACKNOWLEDGMENTS

S.L. and X.M. are thankful for the support from the Office of Naval Research (MURI Grant No. N00014-20-1-2479). P.G.K. acknowledges the support by the U.S. National Science Foundation under the Awards No. PHY-2110030 and No. DMS-2204702. J.Y. is grateful for the support from SNU-IAMD, SNU-IOER, and the National Research Foundation grants funded by the Korea government: Grants No. 2023R1A2C2003705 and No. 2022H1D3A2A03096579 (Brain Pool Plus by the Ministry of Science and ICT).

[1] X. Ni, S. Yves, A. Krasnok, and A. Alù, Topological metamaterials, Chem. Rev. **123**, 7585 (2023).
[2] T. Ozawa, H. M. Price, A. Amo, N. Goldman, M. Hafezi, L. Lu, M. C. Rechtsman, D. Schuster, J. Simon, O. Zilberberg *et al.*, Topological photonics, Rev. Mod. Phys. **91**, 015006 (2019).
[3] H. Xue, Y. Yang, and B. Zhang, Topological acoustics, Nat. Rev. Mater. **7**, 974 (2022).
[4] G. Ma, M. Xiao, and C. T. Chan, Topological phases in acoustic and mechanical systems, Nat. Rev. Phys. **1**, 281 (2019).
[5] H. Huang, J. Chen, and S. Huo, Recent advances in topological elastic metamaterials, J. Phys.: Condens. Matter **33**, 503002 (2021).
[6] E. Lustig, S. Weimann, Y. Plotnik, Y. Lumer, M. A. Bandres, A. Szameit, and M. Segev, Photonic topological insulator in synthetic dimensions, Nature (London) **567**, 356 (2019).
[7] A. Dutt, M. Minkov, I. A. Williamson, and S. Fan, Higher-order topological insulators in synthetic dimensions, Light: Sci. Appl. **9**, 131 (2020).

[8] H. Chen, H. Zhang, Q. Wu, Y. Huang, H. Nguyen, E. Prodan, X. Zhou, and G. Huang, Creating synthetic spaces for higher-order topological sound transport, Nat. Commun. **12**, 5028 (2021).

[9] X. Fan, C. Qiu, Y. Shen, H. He, M. Xiao, M. Ke, and Z. Liu, Probing Weyl physics with one-dimensional sonic crystals, Phys. Rev. Lett. **122**, 136802 (2019).

[10] M. Verbin, O. Zilberberg, Y. Lahini, Y. E. Kraus, and Y. Silberberg, Topological pumping over a photonic fibonacci quasicrystal, Phys. Rev. B **91**, 064201 (2015).

[11] Y. E. Kraus, Y. Lahini, Z. Ringel, M. Verbin, and O. Zilberberg, Topological states and adiabatic pumping in quasicrystals, Phys. Rev. Lett. **109**, 106402 (2012).

[12] Y. Ke, X. Qin, F. Mei, H. Zhong, Y. S. Kivshar, and C. Lee, Topological phase transitions and Thouless pumping of light in photonic waveguide arrays, Laser Photon. Rev. **10**, 995 (2016).

[13] B.-C. Xu, B.-Y. Xie, L.-H. Xu, M. Deng, W. Chen, H. Wei, F. Dong, J. Wang, C.-W. Qiu, S. Zhang *et al.*, Topological Landau-Zener nanophotonic circuits, Adv. Photon. **5**, 036005 (2023).

[14] X. Ni, K. Chen, M. Weiner, D. J. Apigo, C. Prodan, A. Alu, E. Prodan, and A. B. Khanikaev, Observation of Hofstadter butterfly and topological edge states in reconfigurable quasi-periodic acoustic crystals, Commun. Phys. **2**, 55 (2019).

[15] Z. Chen, Z. Chen, Z. Li, B. Liang, G. Ma, Y. Lu, and J. Cheng, Topological pumping in acoustic waveguide arrays with hopping modulation, New J. Phys. **24**, 013004 (2022).

[16] Z.-G. Chen, W. Tang, R.-Y. Zhang, Z. Chen, and G. Ma, Landau-Zener transition in the dynamic transfer of acoustic topological states, Phys. Rev. Lett. **126**, 054301 (2021).

[17] D. J. Apigo, K. Qian, C. Prodan, and E. Prodan, Topological edge modes by smart patterning, Phys. Rev. Mater. **2**, 124203 (2018).

[18] Y. Xia, A. Erturk, and M. Ruzzene, Topological edge states in quasiperiodic locally resonant metastructures, Phys. Rev. Appl. **13**, 014023 (2020).

[19] M. I. N. Rosa, R. K. Pal, J. R. Arruda, and M. Ruzzene, Edge states and topological pumping in spatially modulated elastic lattices, Phys. Rev. Lett. **123**, 034301 (2019).

[20] E. Riva, M. I. N. Rosa, and M. Ruzzene, Edge states and topological pumping in stiffness-modulated elastic plates, Phys. Rev. B **101**, 094307 (2020).

[21] E. Riva, V. Casieri, F. Resta, and F. Braghin, Adiabatic pumping via avoided crossings in stiffness-modulated quasiperiodic beams, Phys. Rev. B **102**, 014305 (2020).

[22] S. Wang, Z. Hu, Q. Wu, H. Chen, E. Prodan, R. Zhu, and G. Huang, Smart patterning for topological pumping of elastic surface waves, Sci. Adv. **9**, eadh4310 (2023).

[23] R. Citro and M. Aidelsburger, Thouless pumping and topology, Nat. Rev. Phys. **5**, 87 (2023).

[24] M. Meloni, J. Cai, Q. Zhang, D. Sang-Hoon Lee, M. Li, R. Ma, T. E. Parashkevov, and J. Feng, Engineering origami: A comprehensive review of recent applications, design methods, and tools, Adv. Sci. **8**, 2000636 (2021).

[25] E. A. Peraza-Hernandez, D. J. Hartl, R. J. Malak, Jr, and D. C. Lagoudas, Origami-inspired active structures: A synthesis and review, Smart Mater. Struct. **23**, 094001 (2014).

[26] Y. Zhu, M. Schenk, and E. T. Filipov, A review on origami simulations: From kinematics, to mechanics, toward multiphysics, Appl. Mech. Rev. **74**, 030801 (2022).

[27] S. Lyu, B. Qin, H. Deng, and X. Ding, Origami-based cellular mechanical metamaterials with tunable Poisson's ratio: Construction and analysis, Intl. J. Mech. Sci. **212**, 106791 (2021).

[28] J. Ji, Q. Luo, and K. Ye, Vibration control based metamaterials and origami structures: A state-of-the-art review, Mech. Syst. Signal Proc. **161**, 107945 (2021).

[29] H. Yasuda, Y. Miyazawa, E. G. Charalampidis, C. Chong, P. G. Kevrekidis, and J. Yang, Origami-based impact mitigation via rarefaction solitary wave creation, Sci. Adv. **5**, eaau2835 (2019).

[30] C. Zhou, B. Wang, J. Ma, and Z. You, Dynamic axial crushing of origami crash boxes, Int. J. Mech. Sci. **118**, 1 (2016).

[31] Y. Miyazawa, C.-W. Chen, R. Chaunsali, T. S. Gormley, G. Yin, G. Theocharis, and J. Yang, Topological state transfer in Kresling origami, Commun. Mater. **3**, 62 (2022).

[32] S. Li, Y. Miyazawa, K. Yamaguchi, P. G. Kevrekidis, and J. Yang, Geometry-informed dynamic mode decomposition in Kresling origami dynamics, Extreme Mech. Lett. **64**, 102082 (2023).

[33] S. Li, P. G. Kevrekidis, and J. Yang, Emergence of elastic chiral landau levels and snake states, Phys. Rev. B **109**, 184109 (2024).

[34] D. Smirnova, D. Leykam, Y. Chong, and Y. Kivshar, Nonlinear topological photonics, Appl. Phys. Rev. **7**, 021306 (2020).

[35] L. J. Maczewsky, M. Heinrich, M. Kremer, S. K. Ivanov, M. Ehrhardt, F. Martinez, Y. V. Kartashov, V. V. Konotop, L. Torner, D. Bauer *et al.*, Nonlinearity-induced photonic topological insulator, Science **370**, 701 (2020).

[36] A. Darabi and M. J. Leamy, Tunable nonlinear topological insulator for acoustic waves, Phys. Rev. Appl. **12**, 044030 (2019).

[37] F. Ma, Z. Tang, X. Shi, Y. Wu, J. Yang, D. Zhou, Y. Yao, and F. Li, Nonlinear topological mechanics in elliptically geared isostatic metamaterials, Phys. Rev. Lett. **131**, 046101 (2023).

[38] P. G. Harper, Single band motion of conduction electrons in a uniform magnetic field, Proc. Phys. Soc. A **68**, 874 (1955).

[39] P. G. Harper, The general motion of conduction electrons in a uniform magnetic field, with application to the diamagnetism of metals, Proc. Phys. Soc. A **68**, 879 (1955).

[40] L. Landau, Zur theorie der energieubertragung. II, Phys. Z. Sowjetunion **2**, 46 (1932).

[41] C. Zener, Nonadiabatic crossing of energy levels, Proc. R. Soc. London A **137**, 696 (1932).

[42] M. Jona-Lasinio, O. Morsch, M. Cristiani, N. Malossi, J. H. Müller, E. Courtade, M. Anderlini, and E. Arimondo, Asymmetric Landau-Zener tunneling in a periodic potential, Phys. Rev. Lett. **91**, 230406 (2003).

[43] S. Flach and C. R. Willis, Discrete breathers, Phys. Rep. **295**, 181 (1998).

[44] See Supplemental Material at http://link.aps.org/supplemental/10.1103/PhysRevB.110.075123 for the simulation setup, topological properties, and nonlinear effect to the topological pumping and time-dependent simulations, which also includes Ref. [45].

[45] H. Yasuda, T. Tachi, M. Lee, and J. Yang, Origami-based tunable truss structures for non-volatile mechanical memory operation, Nat. Commun. **8**, 962 (2017).

[46] D. R. Hofstadter, Energy levels and wave functions of Bloch electrons in rational and irrational magnetic fields, Phys. Rev. B **14**, 2239 (1976).

[47] E. Prodan and Y. Shmalo, The *k*-theoretic bulk-boundary principle for dynamically patterned resonators, J. Geom. Phys. **135**, 135 (2019).

[48] I. Neder, C. Sirote-Katz, M. Geva, Y. Lahini, R. Ilan, and Y. Shokef, Bloch oscillations, Landau-Zener transition, and topological phase evolution in an array of coupled pendula, Proc. Natl. Acad. Sci. USA **121**, e2310715121 (2024).

[49] S. N. Shevchenko, S. Ashhab, and F. Nori, Landau-Zener-Stückelberg interferometry, Phys. Rep. **492**, 1 (2010).

[50] J. Liu, L. Fu, B.-Y. Ou, S.-G. Chen, D.-I. Choi, B. Wu, and Q. Niu, Theory of nonlinear Landau-Zener tunneling, Phys. Rev. A **66**, 023404 (2002).

[51] V. V. Konotop, P. G. Kevrekidis, and M. Salerno, Landau-Zener tunneling of Bose-Einstein condensates in an optical lattice, Phys. Rev. A **72**, 023611 (2005).

[52] M. I. Rosa, M. J. Leamy, and M. Ruzzene, Amplitude-dependent edge states and discrete breathers in nonlinear modulated phononic lattices, New J. Phys. **25**, 103053 (2023).

[53] S.-C. Li, L.-B. Fu, and J. Liu, Nonlinear Landau-Zener-Stückelberg-Majorana interferometry, Phys. Rev. A **98**, 013601 (2018).